Ultrasound Simulation in Bone

Jonathan J. Kaufman, Gangming Luo, and Robert S. Siffert

(Invited Paper)

***Abstract*—The manner in which ultrasound interacts with bone is of key interest in therapy and diagnosis alike. These may include applications directly to bone, as, for example, in treatment to accelerate the healing of bone fractures and in assessment of bone density in osteoporosis, or indirectly in diagnostic imaging of soft tissue with interest in assessing exposure levels to nearby bone. Because of the lack of analytic solutions to virtually every "practical problem" encountered clinically, ultrasound simulation has become a widely used technique for evaluating ultrasound interactions in bone. This paper provides an overview of the use of ultrasound simulation in bone. A brief description of the mathematical model used to characterize ultrasound propagation in bone is first provided. A number of simulation examples are then presented that explain how simulation may be utilized in a variety of practical configurations. The focus of this paper in terms of examples presented is on diagnostic applications in bone, and, in particular, for assessment of osteoporosis. However, the use of simulation in other areas of interest can easily be extrapolated from the examples presented. In conclusion, this paper describes the use of ultrasound simulation in bone and demonstrates the power of computational methods for ultrasound research in general and tissue and bone applications in particular.**

I. Introduction

The use of computer simulation is a common tool in a variety of engineering disciplines and problems. The most common applications include structural and electromagnetic analyses. The expansion of simulation methods to ultrasound applications appeared relatively late (largely in the 1990s) compared with the two above-mentioned fields. This was due primarily to the extremely high degree of computational overhead associated with ultrasound simulation. However, the advent of more and more powerful desktop computers has enabled the expansion of simulation methods to the field of ultrasound as well.

Manuscript received June 7, 2007; accepted November 9, 2007. The support of the National Institute of Arthritis and Musculoskeletal and Skin Diseases (Grant Number 1R44 AR054307), the National Institute on Aging (Grant Number 1R43 AG027722), and the National Center for Research Resources (Grant No. 1R43 RR16750) of the National Institutes of Health, through the Small Business Innovative Research Program, the Carroll and Milton Petrie Foundation, and the generosity of interested donors, are all gratefully acknowledged.

J. J. Kaufman and R. S. Siffert are with the Department of Orthopedics, The Mount Sinai School of Medicine, New York, NY.

J. J. Kaufman and G. M. Luo are with CyberLogic, Inc., New York, NY (e-mail: jjkaufman@cyberlogic.org).

G. M. Luo is also with the Veterans Administration (VA) New York Harbor HealthCare System, VA Hospital, New York, NY, and the Department of Rehabilitation Medicine, New York University School of Medicine, New York, NY.

Digital Object Identifier 10.1109/TUFFC.2008.784

A strong motivating factor for development of ultrasound simulation methods in bone has been the interest in diagnosing osteoporosis. Osteoporosis is a significant health problem affecting more than 20 million people in the United States and more than 200 million worldwide [1]. Osteoporosis is defined as the loss of bone mass with a concomitant disruption in microarchitecture, leading to an increased risk of fracture [2]. The most common osteoporotic fractures occur at the wrist, spine, and hip. Hip fractures have a particularly negative impact on morbidity. Approximately 50 percent of those individuals suffering a hip fracture never live independently again [3]. Currently, there are about 200 thousand hip fractures yearly in the United States and approximately one million worldwide [1], [4]. The aging of the worldwide population is expected to increase the incidence of hip and other fractures as well [1].

The primary method for diagnosing osteoporosis and associated fracture risk relies on bone densitometry to measure bone mass [5]. The use of bone mass is based on the well-established thesis that bone strength is strongly related to the amount of bone material present and that a stronger bone in a given individual is associated generally with a lower fracture risk [6]. Indeed, it has been shown that bone mass has about the same predictive power in predicting fractures as blood pressure has in predicting strokes [2].

Inherent strength of bone depends upon a host of multifactorial components, the amount of mineralized matrix being a major factor. Radiological densitometry, which measures the (areal) bone mineral density (BMD) at a given site (e.g., hip, spine, forearm) is currently the accepted indicator of bone strength and fracture risk [6], [7]. Clinically, this is often done using dual energy x-ray absorptiometry (DXA), which measures the BMD in units of grams per square centimeter [7].

Notwithstanding the fact that x-ray methods are useful in assessing bone mass and fracture risk, osteoporosis remains one of the largest undiagnosed and underdiagnosed diseases in the world today [1]. Among the reasons for this is that densitometry (i.e., DXA) is not a standard tool in a primary care physician's office. This is due to its expense and inconvenience, and reticence among patients concerning x-ray exposure, particularly in young adults and children.

Ultrasound has been proposed as an alternative to DXA for a number of reasons. These include the facts that it is non-ionizing, relatively inexpensive, and simple to use. Moreover, since ultrasound is a mechanical wave and inter-

acts with bone in a fundamentally different manner than X-rays, it may be able to provide additional components of bone strength, notably its trabecular architecture [8], [9].

Because, as already noted, analytic solutions to propagation in bone with its associated irregular geometry and heterogeneous character are not available, research studies had until the 1990s been mainly based on experimental data, both *in vitro* and clinical. However, the development of ultrasound simulation software has enabled a broad range of questions to be addressed, as the following sections will demonstrate. This paper provides an overview of the use of ultrasound simulation in bone. A brief description of the mathematical model used to characterize ultrasound propagation in bone is first provided. A number of examples are then presented that explain how simulation may be utilized in a variety of practical configurations. A discussion and conclusion section ends the paper.

II. Analytic Basis for Ultrasound Simulation

The fundamental equation characterizing the three-dimensional (3-D) linear propagation of ultrasound in a homogeneous medium comprised of an isotropic material with viscous loss is provided by the following visco-elastic wave equation [10], [11]:

$$\rho\frac{\partial^2\mathbf{u}}{\partial t^2}=\left(\mu+\eta\frac{\partial}{\partial t}\right)\nabla^2\mathbf{u}+\left(\lambda+\mu+\xi\frac{\partial}{\partial t}+\frac{\eta}{3}\frac{\partial}{\partial t}\right)\nabla\nabla\cdot\mathbf{u}. \tag{1}$$

In (1), $\mathbf{u}=\mathbf{u}(x, y, z, t)$ is the time-varying displacement vector which is a function of the Cartesian coordinates x, y, and z, and has scalar components u_x, u_y, and u_z, respectively; ρ is the mass density; λ and μ are the first and second Lamé constants, respectively; η and ξ are the first and second viscosities, respectively; and t is time. Eq. (1) models only the linear propagation of ultrasound in a medium. In general, (1) must be solved with respect to the boundary conditions of a given object, which also includes the input source(s) that have prescribed time-dependent displacements (or stresses) at a given location, as well as a set of initial conditions. It should be noted that (1) models material losses by a viscous loss mechanism [11]; however, other types of loss mechanisms may exist and would need to be modeled appropriately [10].

A set of dispersion relations can be associated with (1) that allows the frequency-dependent velocities and attenuations (longitudinal and shear) associated with a given homogeneous material to be computed. In particular, the longitudinal and shear velocities v_L and v_s, respectively, and longitudinal and shear attenuations, α_L and α_s, respectively, may be expressed as

$$v_L=\sqrt{\frac{(\lambda+2\mu)^2+\left(\xi+\frac{4}{3}\eta\right)^2\omega^2}{\rho}}\cdot\frac{\sqrt{2}}{\sqrt{(\lambda+2\mu)+\sqrt{(\lambda+2\mu)^2+\left(\xi+\frac{4}{3}\eta\right)^2\omega^2}}}, \tag{2a}$$

$$v_S=\sqrt{\frac{(\mu^2+(\eta\omega)^2}{\rho}}\frac{\sqrt{2}}{\sqrt{\mu+\sqrt{\mu^2+(\eta\omega)^2}}}, \tag{2b}$$

$$\alpha_L=\frac{\omega^2}{\sqrt{2}}\sqrt{\frac{\rho}{(\lambda+2\mu)^2+\left(\xi+\frac{4}{3}\eta\right)^2\omega^2}}\cdot\frac{\left(\xi+\frac{4}{3}\eta\right)}{\sqrt{(\lambda+2\mu)+\sqrt{(\lambda+2\mu)^2+\left(\xi+\frac{4}{3}\eta\right)^2\omega^2}}}, \tag{2c}$$

$$\alpha_S=\frac{\eta\omega^2}{\sqrt{2}}\sqrt{\frac{\rho}{(\mu^2+(\eta\omega)^2}}\frac{1}{\sqrt{\mu+\sqrt{\mu^2+(\eta\omega)^2}}}. \tag{2d}$$

Note the approximately frequency-squared behavior of the attenuation functions [(2c)–(2d)] for "low" frequencies; this is a result of the viscous loss model assumed in (1). Other loss models would, in general, lead to other frequency-dependent behavior in (2a)–(2d).

As noted, (1) is applicable to a homogeneous object only; for heterogeneous propagation mediums such as bone, the propagation in each distinct *homogeneous* region (e.g., marrow) must be solved according to (1). The conditions for the stresses and strains at the interfaces between all of the distinct regions must also be satisfied [10], [11]. Many different numerical methods can be used for obtaining solutions to the lossy elastic wave equation [e.g., finite difference time domain (FDTD) or finite element methods (FEM)]. In addition, a broad range of specific implementations within a given method can be implemented (e.g., an explicit or implicit approach). In this paper, little attention is given to the details of the simulation method and implementation in order to focus on the main topic, namely, the use of simulation for studying ultrasound propagation in bone. Reference to the specific methods and implementations used in the simulations presented in this paper will, however, be provided.

III. Ultrasound Computer Simulation Examples

The first simulation is part of a study designed to develop a new system for estimating the bone mineral density at the distal radius [12]. A set of 6 plastic rods and 7 plastic tubes designed to validate the results of simulations were measured empirically. A 3.5-MHz 12.7-mm-diameter source and 1.5-mm-diameter receiver in a through-transmission configuration were used within a water tank, between which the plastic or bone samples were placed. The received waveform was stored for subsequent processing. This configuration, as shown in Fig. 1, is similar to the one described by Robinson and Greenleaf [13]. The nominal wavelengths (velocities) at 3.5 MHz were 0.8 mm (2700 m/s) in the plastic and 0.4 mm (1500 m/s) in water.

A set of 13 two-dimensional (2-D) ultrasound simulations of analogous models was also carried out [14]–[16]. Each simulation used a source waveform and configuration

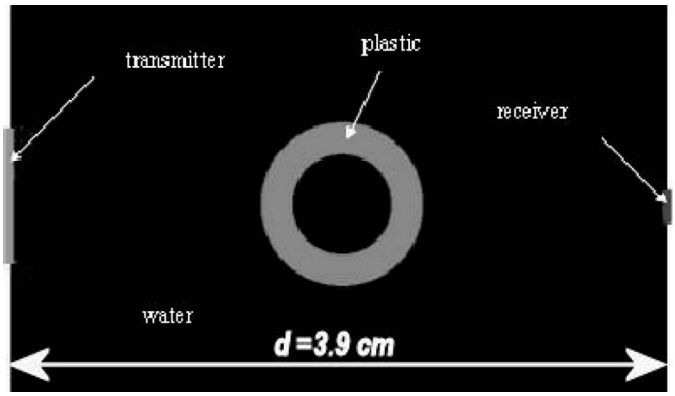

Fig. 1. Schematic setup of tube and rod validation study.

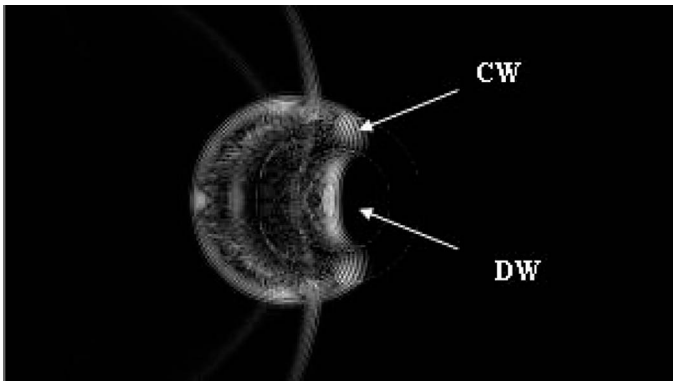

Fig. 2. The ultrasound wave propagating (from left to right) through a plastic tube showing a snapshot of the displacement magnitude at $t = 30.9$ μs. Reprinted from *Acoustical Imaging*, vol. 29, 2008, Kaufman J. J., Luo, G. M., Blazy B., Siffert R. S., "Quantitative Assessment of Tubes and Rods: Comparison of Empirical and Computational Results," with kind permission of Springer Science and Business Media.

similar to those used in the experimental measurements. A typical simulation at a given point in time ($t = 30.9$ μs) for a tube is shown in Fig. 2. The grey level displayed is proportional to the magnitude of the displacement at that location. The interfaces between water and the plastic of the tube are also shown. The notations "CW" and "DW" denote circumferential wave and direct wave, respectively; there are waves that propagate through distinct portions of the tube before arriving at the receiver. The CW travels only within the tube itself, while the DW travels through the walls and also through the inner water-filled portion of the tube.

The receiver waveform produced by the simulation for the tube of Fig. 2 is shown in Fig. 3.

The ultrasound data obtained from both the bench-top experiments and the computer simulations were processed to obtain an ultrasound parameter known as *net time delay* (NTD), associated with each sample. The NTD is the difference between the times of travel of waveforms with and without the rod or tube in the path, i.e., with water only and with water and sample, and has been shown to be a measure of the thickness of the material (e.g., plastic)

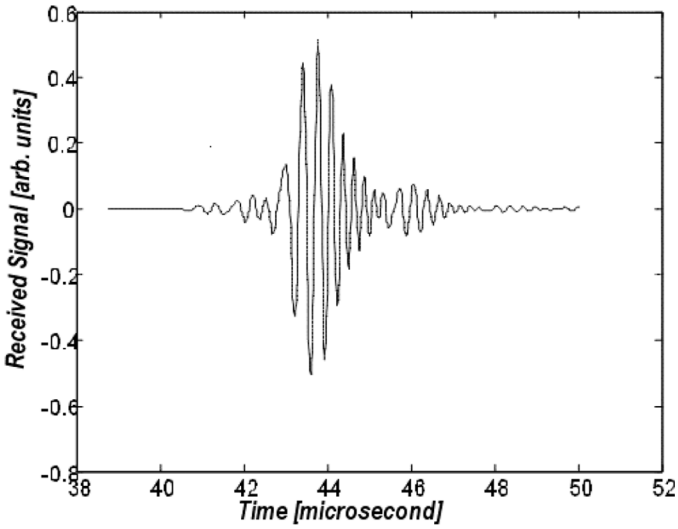

Fig. 3. The simulated receiver signal for a tube.

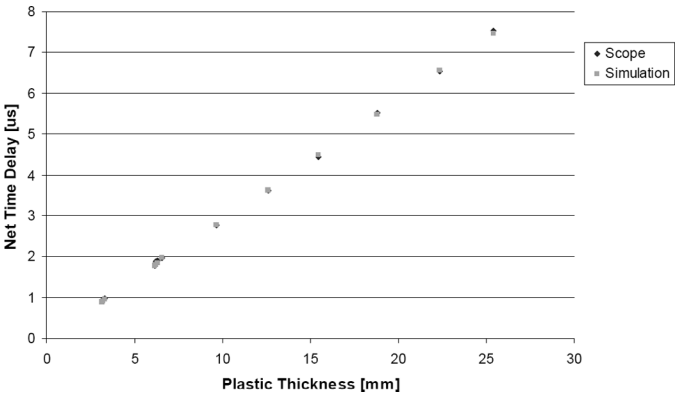

Fig. 4. Comparison of the NTD vs. plastic thickness for the simulated and the scope data. Reprinted from *Acoustical Imaging*, vol. 29, 2008, Kaufman J. J., Luo, G. M., Blazy B., Siffert R. S., "Quantitative Assessment of Tubes and Rods: Comparison of Empirical and Computational Results," with kind permission of Springer Science and Business Media.

through which the ultrasound wave has propagated [17]. Here, travel time is defined as the time at which the second peak of the given portion (i.e., the CW or DW portion) of the signal arrives at the receiver. The estimation of plastic thickness using the NTD is based on the arrival time of the DW only.

The correlation of NTD with plastic thickness for both the empirical and the simulated data is shown in Fig. 4. Note that the definition of plastic thickness is the diameter for the rods and twice the wall thickness for the tubes. As may be seen, there is extremely close correspondence between the simulated and the empirical results, which provides a good demonstration of validation of the simulation. Moreover, both the empirical and the simulated results demonstrate correlations of NTD with plastic thickness greater than 0.99.

A set of ultrasound simulations was then carried out on a set of radial bones. The cross sections of 20 commer-

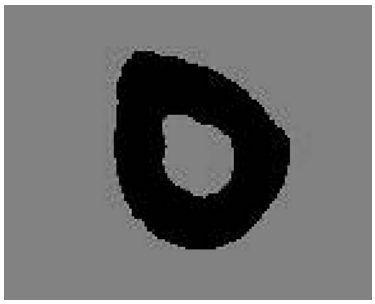

Fig. 5. Cross section of a radial bone.

cially obtained (Skulls International, Tulsa, OK) human radii were photographed and digitized into images that would serve as the basis for the simulations. The cross section was selected at approximately the "1/3" location [18]. Fig. 5 displays a typical digitized cross section. The "cortical thickness" was defined by the sum of the thicknesses of the posterior and anterior cortices. Each thickness was defined as the average thickness over a 1-mm-wide region located at the center of the medullar cavity.

Ultrasound propagation was simulated through the set of 20 radial bone images. A set of three images showing the propagating wave at three instants in time is shown in Fig. 6(a)–(c). A typical received waveform associated with a radial cross section is shown in Fig. 7. There are three identifiable portions of this waveform. The earliest arriving signal is that associated with the CW, the second portion is that associated with the DW, and the third portion is the signal that has propagated primarily through water only ("WW"), as the propagating waveform from the single large element source that is in the water is "shadowed" by the radius but not negligible.

The NTD delay was computed using the simulated received signals for all of the radial bones. These data were then compared to the measured overall cortical thickness. As may be seen in Fig. 8, there is high correlation ($R = 0.99$) between the NTD and the thickness.

This first simulation serves to highlight certain key aspects that may at first not be readily apparent. First, it is important to point out that the results obtained (i.e., Fig. 8) were from hundreds, if not thousands, of simulations in a "trial and error" framework. These computational simulations were used to determine a number of key "system characteristics." These included, for example, frequency, bandwidth, and signal shape associated with the source and receiver in a through-transmission configuration, as well as the size of receiver and how many measurements (in a spatial sense) would be needed to identify the different portions of the waveform. This is related to the number, pitch, and size of elements of the array receiver that gave the best results in terms of being able to estimate bone thickness. In addition, the simulations were also used to identify the sensitivity that various parameters had on the ultimate results. These included the effect of rotation (of the bone around its long axis) and changes in velocity of ultrasound in bone and soft tissue. This brings to the fore

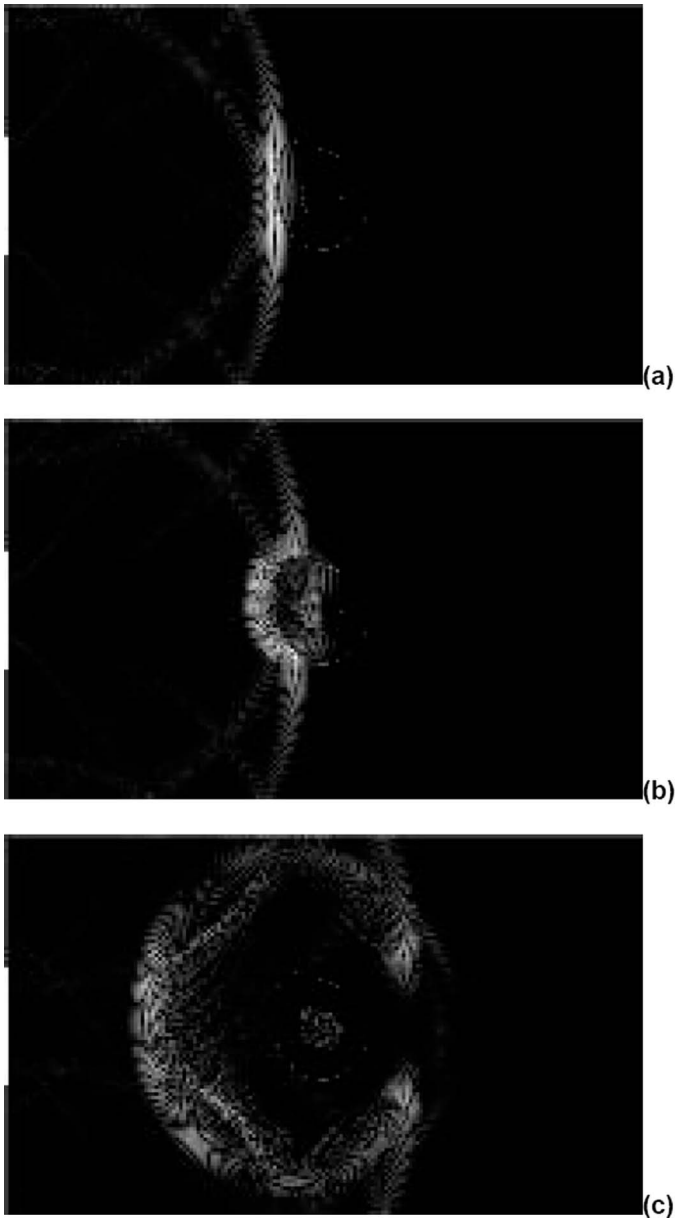

Fig. 6. The ultrasound wave propagating through the radius cross section shown in Fig. 5, showing, from top to bottom, snapshots of the displacement magnitude at times = (a) 21.3 μs; (b) 22.8 μs; and (c) 31.3 μs.

another key aspect of simulation: It allows one to do "experiments" that are either extremely difficult or, in fact, completely impossible. In the present instance, the difficult aspects are, for example, related to the use of many simulations (that can, it should be noted, run in a "batch mode" "24/7") that would take many more weeks or months to do as bench-top experiments. Furthermore, the simulations that tested different frequencies, array designs, and transducer sizes, among other system considerations, besides taking an extremely long time, would also be prohibitively expensive in terms of fabrication costs. These are all the "difficult" parts associated with empirical measurements but that are made entirely feasible in simulation. Later we will discuss the "impossibility" of certain kinds of exper-

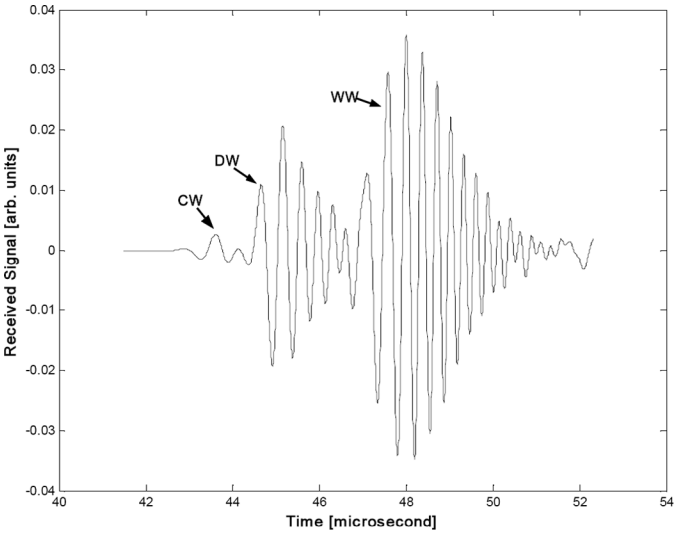

Fig. 7. The simulated ultrasound signal for the radial bone of Fig. 5.

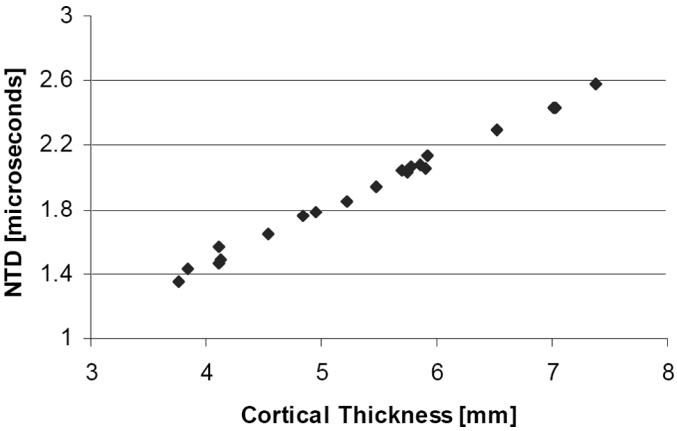

Fig. 8. Estimation of bone thickness for the 20 radii using the net time delays associated with the simulated ultrasound data.

iments, but which can be done quite straightforwardly in simulation.

The next simulation is a 3-D one that illustrates how an ultrasound wave may be visualized as it propagates through bone. Although it is difficult to display here, the array of images below (Fig. 9) shows a 3-D simulation of the propagation of an ultrasound 1-MHz broadband pulse through a small section (1 cm long) of the mid-shaft of a proximal phalanx (finger bone). The image of the bone was obtained using micro-computer tomography (micro-CT). The sequence of images shows the wave as it travels from right to left and through the bone. In the last frame, two earliest arriving waves can be discerned which may correspond to the CW and DW, respectively, of the previous (2-D) simulation.

Another example explores the use of another ultrasound parameter, known as the mean frequency (MF), in assessing architectural differences above and beyond that represented by mass alone. The MF is closely related to the more well-known broadband ultrasound attenuation (BUA) parameter [16]. Generally, the higher the BUA, the lower the MF, representing the loss in higher frequencies when passing through bone characterized by an attenuation with a higher slope or BUA. The MF is presumed (like the BUA) to be dependent on the number of trabecular surfaces in the bone, which is responsible at least in part for scattering the ultrasound. The relative degree of heterogeneity may also affect the MF (and the BUA) [9], [16]. In this simulation, two (2-D) bone images obtained with micro-CT were utilized, as shown in Fig. 10: a trabecular slice [Fig. 10(a)] and a cortical slice [Fig. 10(b)] from the distal and midshaft portions of a proximal phalanx, respectively. The cortical bone was thinned using morphological image processing (erosions) in order to produce approximately equal mean bone thicknesses in both bone slices. An ultrasound wave was then simulated through each slice and the NTD and the MF computed. Table I shows the results. As may be seen, the NTD is relatively unchanged as it reflects mainly the mean bone thickness (about the same for both cases). However, the MF is about 80 percent different in the two cases, reflecting the fact that the architecture of the two cases is very distinct. This simulation should help show that simulation can explore key aspects of ultrasound bone assessment, namely, to examine the sensitivity of various ultrasound parameters to bone mass, architecture, geometry, and material properties per se, for ultimately noninvasively evaluating the strength and fracture risk of bone.

TABLE I
ULTRASOUND PARAMETERS IN CORTICAL AND TRABECULAR BONE.

Phalanx	Bone thickness (mm)	NTD (μs)	MF (MHz)
Cortical	2.34	0.60	0.83
Trabecular	2.33	0.69	0.45

Another simulation involving primarily trabecular bone was carried out on a set of 3-D bone images [17]. In this study, a 1.2-cm-diameter core was drilled from the posterior region of 25 human calcanei, obtained from a commercial supplier (Evolution, New York, NY). They were then scanned with micro-CT at 40 μm resolution, and each 3-D image voxel was segmented into either bone or soft tissue using simple thresholding. An example of one scanned and segmented calcaneal core is shown in the volume-rendered image in Fig. 11. Note that the cylinder consists mostly of trabecular bone, but also includes the thin cortical shells. Each segmented image was processed in the medial-lateral direction to obtain the bone mineral density in grams per square centimeter, the same data as would be determined by DXA. Each 3-D image served as the basis for simulating the propagation of a 1-MHz broadband pulse through it along the medial-lateral direction. The ultrasound waveform was input by placing a circular source transducer over the entire face of one end of the cylinder, separated from the cortical shell by a small layer of water (2–4 mm). At the other end, a circular receiver was placed, also sepa-

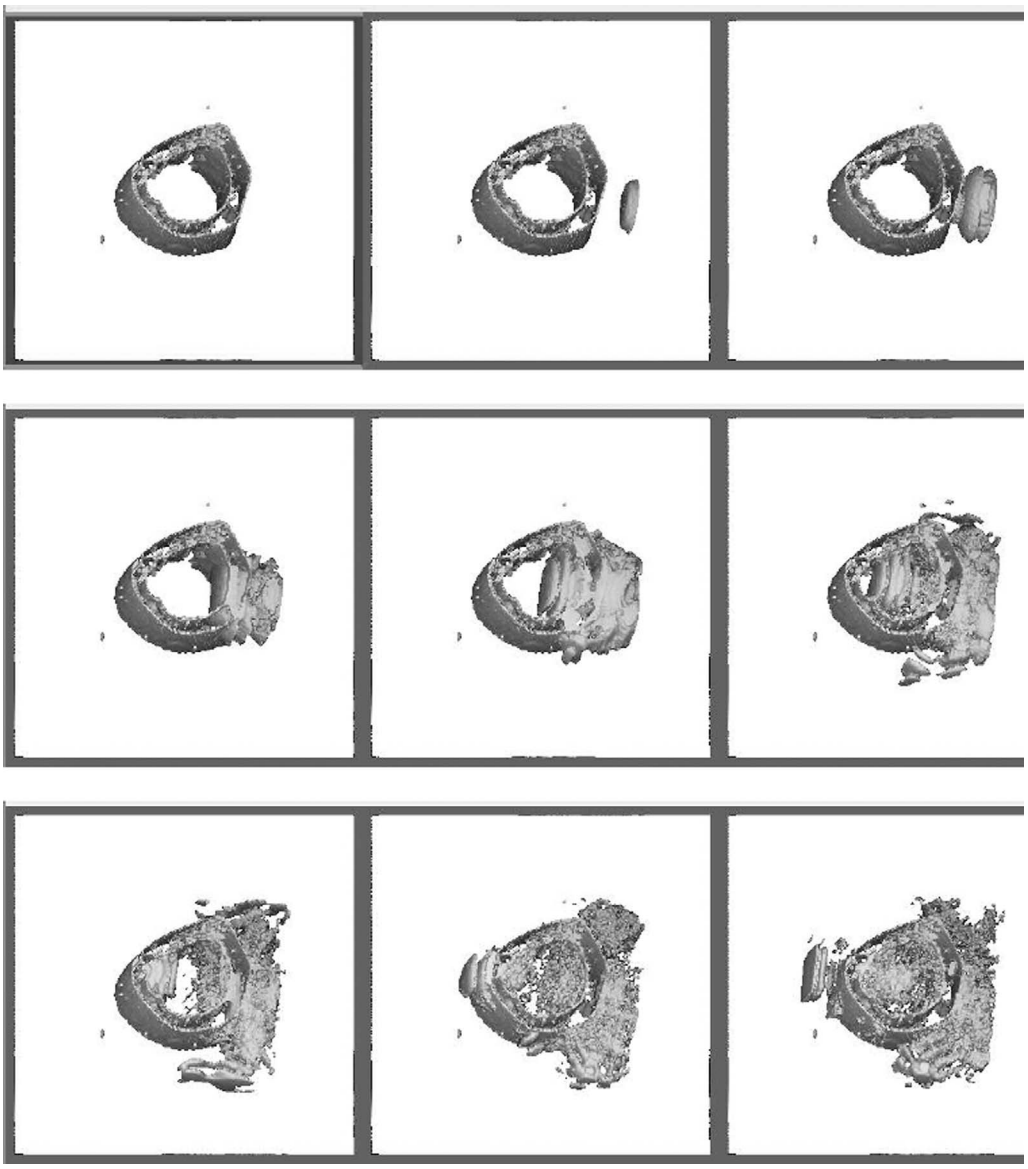

Fig. 9. The images show a broadband 1-MHz ultrasound wave as it propagates through the midshaft of a proximal phalanx of 1 cm in length. The images are sequential in time and proceed in each row from left to right as time increases.

Fig. 10. (a) Trabecular bone slice from the distal portion of a proximal phalanx, (b) Cortical bone slice from the midshaft portion of a proximal phalanx.

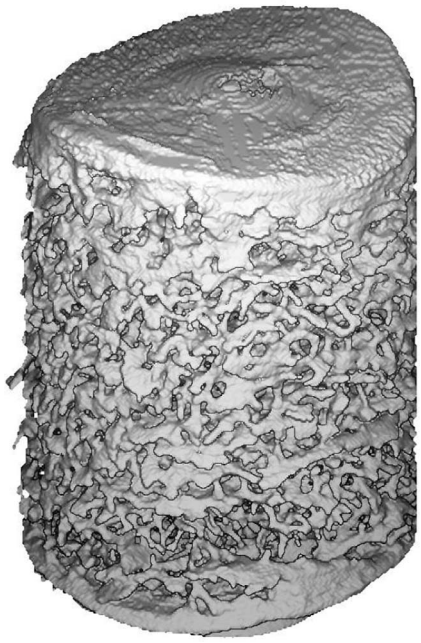

Fig. 11. Rendered image of a micro-CT scan of a human calcaneal bone core. Reprinted from *Ultrasound in Medicine and Biology*, vol. 33, Kaufman J. J., Luo G. M., Siffert R. S., "A portable real-time ultrasonic bone densitometer," pp. 1445–1452, Copyright (2007), with permission from Elsevier.

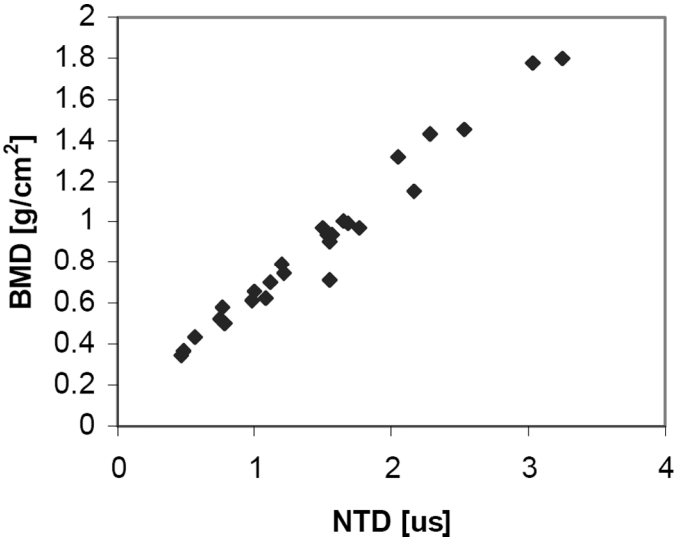

Fig. 12. BMD vs. NTD determined from computer simulations of ultrasound propagation through 25 calcaneal images. Reprinted from *Ultrasound in Medicine and Biology*, vol. 33, Kaufman J. J., Luo G. M., Siffert R. S., "A portable real-time ultrasonic bone densitometer," pp. 1445–1452, Copyright (2007), with permission from Elsevier.

rated from the cortical bone by 2–4 mm of water and also covering the entire face. The NTD was computed for each sample and compared with the mean BMD (Fig. 12). As may be seen, the NTD is extremely highly correlated with bone mass with an R-squared value of approximately 0.99.

An interesting set of simulations was presented by Bossy *et al.* in [19]. In this study, simulation was used to study the axial propagation of ultrasound in cortical bone models. Although a great deal of theory has been developed for specialized geometries (e.g., 2-D isotropic plates), the situation for cortical bone is much more complex, and no analytic solutions are available. The principal benefit of axial propagation is that it affords the potential for determining both cortical thickness and the velocity of ultrasound in bone, which itself can be an indicator of mineralization, among other material property factors. Since both material properties and cortical thickness are related to bone strength, the axial method has been the subject of much research and development. The method also has the advantages that it can be applied to many bones (e.g., tibia, radius, ulna) with access needed on only one side of a limb. Fig. 13 shows the specific configuration used for these axial transmission measurements, although many other configurations can be used.

Fig. 14 shows the results of a simulation for a simpler problem, a 2-D cortical bone plate. As may be seen from even this 2-D simulation, the propagation of an ultrasound wave is extremely complex in such structures. The utility of simulation for analyzing ultrasound modes of propagation and determining bone properties of interest should be obvious, given the even more complex situation in 3-D.

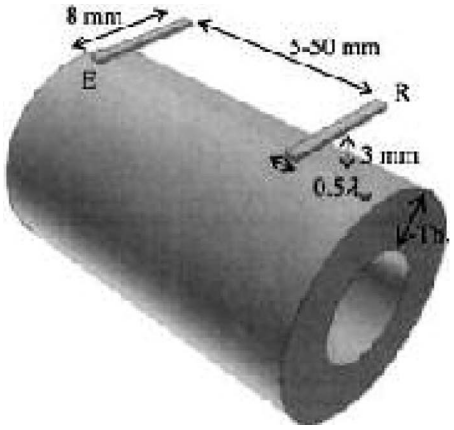

Fig. 13. Typical 3-D measurement configuration involved in axial transmission on cortical bone, where λ_w is the wavelength in water. The elements are $\lambda_w/2$ in width; E: emitter; R: receiver(s); Th: cortical thickness. Reused with permission from E. Bossy, M. Talmant, and P. Laugier , *The Journal of the Acoustical Society of America*, *115*, 2314, (2004). Copyright 2004, Acoustical Society of America.

Another study by the same group examined by simulation the relationship of volume fraction, mineralization, and structure to broadband ultrasound attenuation and speed of sound (SOS) [20]. In this comprehensive study by Haïat *et al.*, 30 human femur specimens served as a base from which a total of 164 "specimens" were obtained through morphological image processing (erosions and dilations) of their associated micro-CTs. One original actual specimen together with two images derived by erosion and dilation, respectively, are shown in Fig. 15.

The velocities (SOS) and attenuations (BUA) of the 164 sample images were used in a finite difference simulation to evaluate the received waveform in a through-

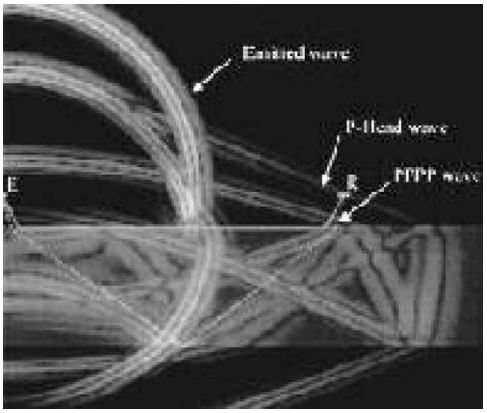

Fig. 14. Snapshot of 2-D wave propagation on a cortical bone plate. The propagation is highly dependent on both the thickness of the plate and its material properties. In a 3-D case with real bone, it would also be dependent on the specific geometry of the bone. Reused with permission from E. Bossy, M. Talmant, and P. Laugier , *The Journal of the Acoustical Society of America*, *115*, 2314, (2004). Copyright 2004, Acoustical Society of America.

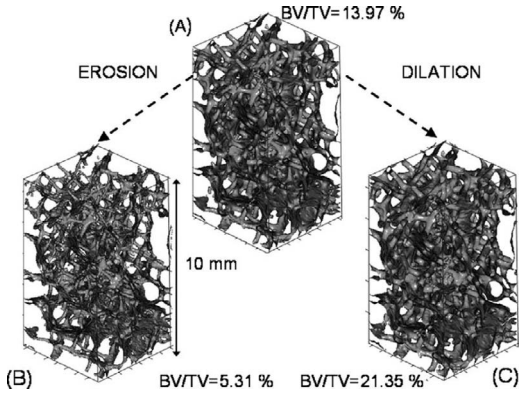

Fig. 15. Illustration of the morphological image processing alterations. Images represent the 3-D trabecular structures: (A) original sample; (B) eroded structure; and (C) dilated structure. Reproduced from *J Bone Miner Res* 2007; 22: 665–674 with permission of the American Society for Bone and Mineral Research.

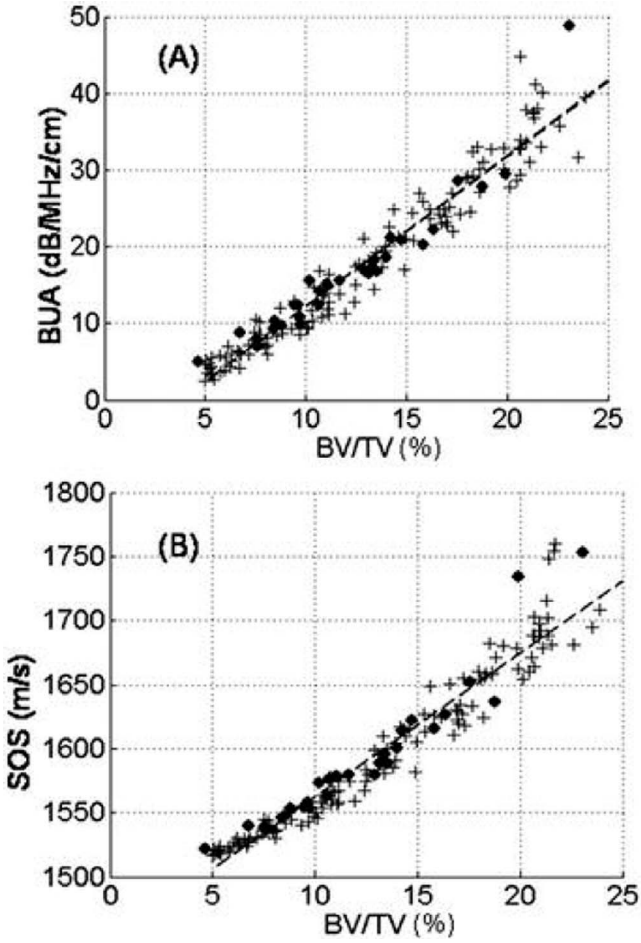

Fig. 16. Variations of (A) the BUA and (B) the SOS as a function of bone volume/total volume (BV/TV) obtained from numerical simulations of ultrasonic propagation through 164 3-D structures. Quantitative ultrasound (QUS) parameters for the original (unaltered) models ($N = 30$) and for the 134 derived structures are indicated by black dots and crosses, respectively. The dots and crosses correspond, respectively, to the original structures obtained from the micro-CT and to the structures modified with the image processing algorithm (dilation and erosion procedures). The dotted lines in both figures correspond to a linear fit approximation. Reproduced from *J Bone Miner Res* 2007; 22: 665–674 with permission of the American Society for Bone and Mineral Research.

transmission configuration. Propagation was carried out orthogonal to the sagittal plane (anteroposterior), and each received waveform was used to compute the associated SOS and BUA. Fig. 16 presents the results and shows the excellent correspondence between bone volume fraction and the two parameters. It should be noted that in this simulation all 134 samples were assumed to have the same density and elastic constants. This study also analyzed the effects on the BUA and the SOS of both material property and architectural changes. In general, it was reported that the strongest factor affecting the BUA and the SOS were volume fraction, although both material property and architecture did play a significant role as well. This was particularly the case when the volume fraction was low.

The previously presented simulations were for experiments which could, at least in principle, be carried out *in vitro*, although for practical reasons it would require extremely inordinate amounts of time and resources. However, there are also simulations which may be useful to do and which cannot be empirically carried out at all. One such simulation has been presented by Bossy *et al.* [21]. In this study, the effect of the shear component that arises in bone on normalized attenuation (nBUA) was studied. This involved two simulations, one with actual bone whose first and second Lamé constants were non-zero, and the second simulation where the shear modulus was set to zero and the first Lamé constant adjusted so that the longitudinal velocity remained the same as in the first simulation. Thus, these two simulations allowed the determination of the effect of mode conversion on the measured normalized attenuation. Fig. 17 displays the results for the two simulations; they were carried out on a set of micro-CT images of 31 cancellous bone specimens machined from 31 human

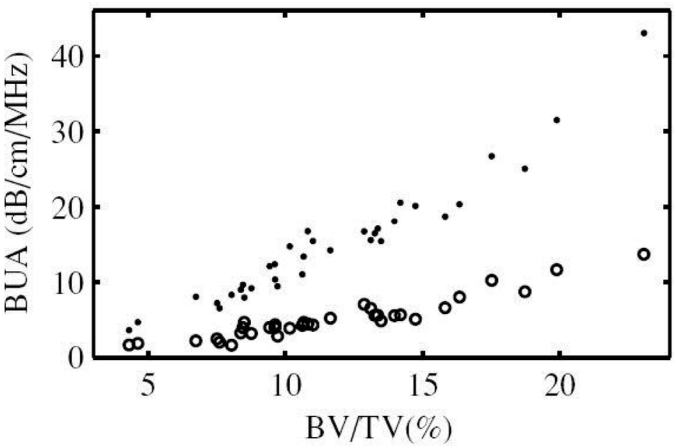

Fig. 17. Simulated nBUA values versus bone volume fraction for bone modeled as a solid structure (dots) and fluid structure (circles). Modeling bone as a fluid reduces nBUA values by approximately a third. Reprinted with permission from *Physics in Medicine and Biology*, Bossy E., Padilla F., Peyrin F., Laugier P., Three-dimensional simulation of ultrasound propagation through trabecular bone structures by synchrotron microtomography, 2005; *50*:5545–5556.

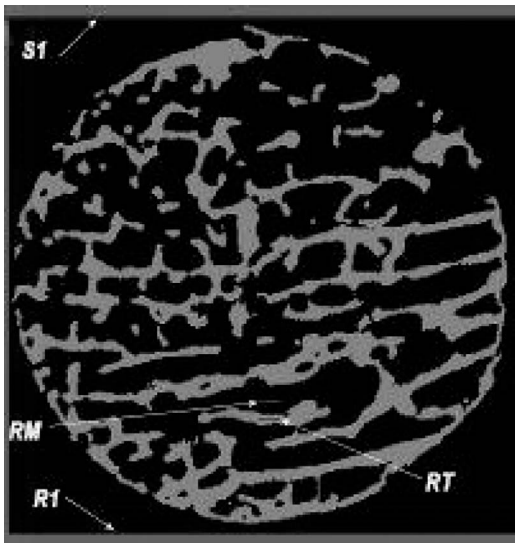

Fig. 18. A slice of trabecular bone taken from a core in the posterior portion of the human calcaneus in the medial-lateral direction. The locations of the source transducer (S1), the through-transmission receiver transducer (R1), and two small receivers located entirely within a trabecula (RT) and within a marrow space (RM), respectively, are shown.

femora. It may immediately be seen that mode conversion and shear waves account for a large part of the observed variation, reducing the shear-free BUA values by about a third.

Another simulation "impossible" to carry out in practice but which may provide useful information is one in which a receiver is placed within a trabecula. This may be done, for example, to characterize the amount of acoustic energy deposited within a portion of trabecular bone tissue. Fig. 18 displays a slice of trabecular bone taken from a micro-CT-imaged 1.2-cm-diameter core in the posterior portion of the human calcaneus in the medial-lateral direction (as in Fig. 11). Fig. 18 also shows the location of a source transducer (S1), a through-transmission receiver transducer (R1), both of which cover the entire face of their respective sides, and two small (0.6 mm) receivers located entirely within a trabecula (RT) and within a marrow space (RM). Fig. 19 displays a set of four "snapshots" of the propagating wave at four instants of time. As may be seen, there are two components of the wave, a ballistic component and a scattered component. The interfaces between the trabeculae and marrow spaces are also shown. The two waveforms associated with the two receivers RT and RM are shown in Fig. 20. Perhaps somewhat surprisingly, the signal levels within the marrow and within a trabecula at this location are on the same order. This may be due to the coupled nature of the acoustic field and the relatively large wavelength with respect to the dimensions of a single trabecula. Note also the high amount of scattering that exists after the ballistic portion of the signal has passed through (the source signal is only 3 μs in length). The received signal at the single large receiver is shown in Fig. 21. It is particularly interesting to note that the coherent averaging at the large receiver has reduced quite dramatically the amount of scatter in the signal after the ballistic portion of the waveform.

Another simulation example serves to illustrate another application of ultrasound in bone, namely, its use for assessment of fracture healing. Fracture healing assessment is part art, part science, and somewhat subjective, so it would be helpful to have an objective tool for providing additional information over and above that provided by radiological and clinical measures [5], [22]. To this end, ultrasound has been proposed, as early as 1958, to assess fracture healing, although there is still no effective method in use [23], [24]. Simulation has recently begun to assist in this development, as, for example, in a study reported by Dodd *et al.* [25]. A similar study was also reported by Protopappas *et al.* [26]. Fig. 22 displays their experimental setup, in which both a fixed source and a receiver that is progressively moved across the fracture site in an axial transmission configuration are shown.

Simulation was used to analyze the propagation of ultrasound as a function of gap size and transducer separation. Fig. 23 shows the propagating wave at an instant in time. These snapshots are negative images of the simulations presented throughout the rest of this paper; therefore, successive dark and light regions of the waves represent high and low pressure regions in a material, respectively, with black corresponding to the highest pressure and white the lowest. The thin grey lines at the top of each picture represent an overlapping array of receiving transducers. Analysis of the so-called "first arriving signal" or FAS in simulation has been correlated with the fracture gap size and may ultimately lead to a new objective measurement device for fracture healing assessment [25], [26]. Note that the kind of model used here in the simulation would also be useful for analyzing the exposure levels in bone, which is an important consideration both

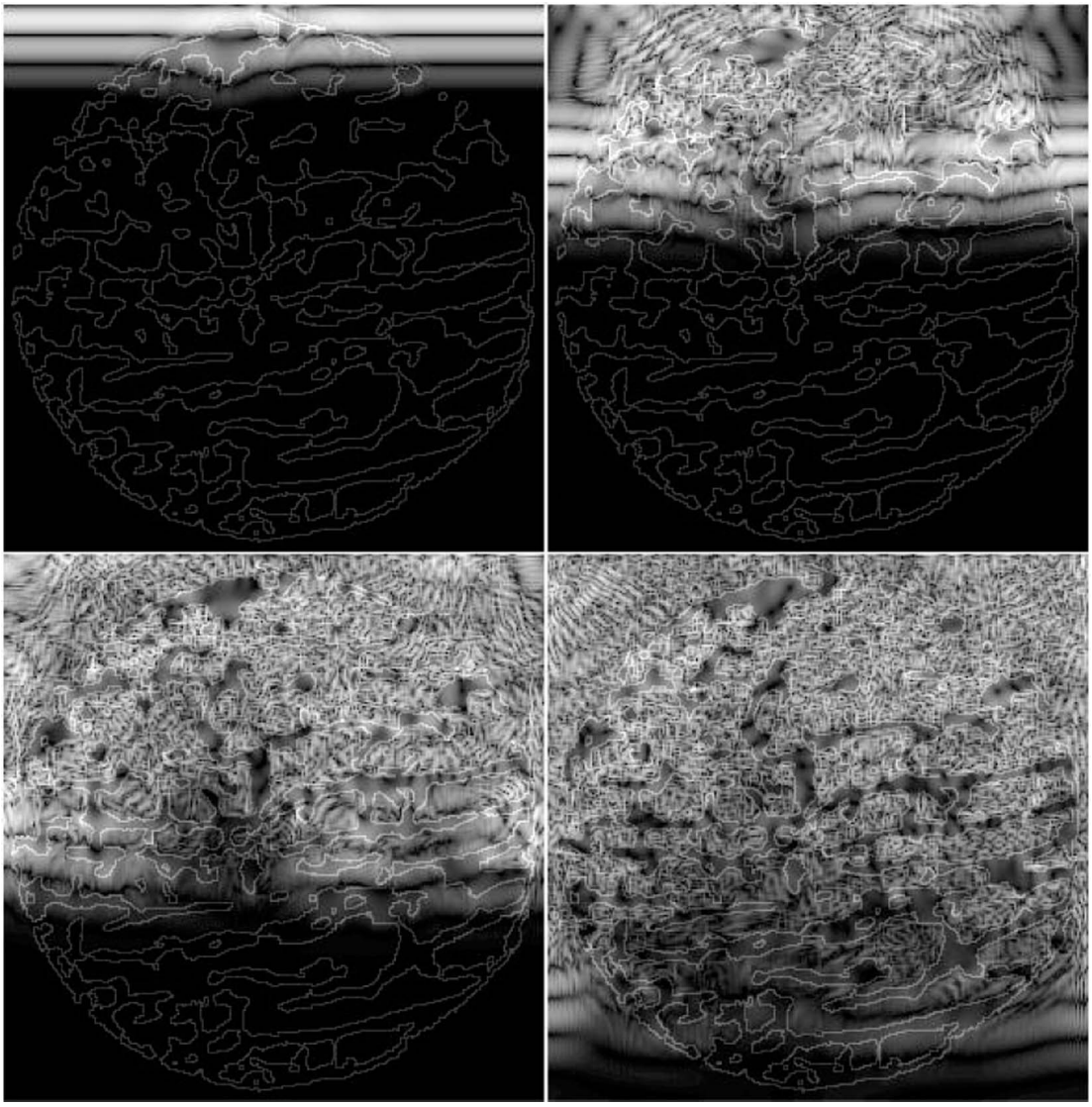

Fig. 19. The propagating wave at four instants of time. As may be seen, there is a strong ballistic component and an equally strong scattered component.

in physical therapy and in bone fracture healing therapy applications, to ensure safety and efficacy.

It is also useful to at least mention another application of simulation in bone. Aubry *et al.* [27] used simulation in the development of a system for minimally invasive brain surgery by high-intensity focused ultrasound beams. Because the skull induces strong aberrations both in phase and amplitude, severe degradations in beam shape can occur. High resolution CT scans were used in conjunction with simulations; the set of signals to be emitted by elements of an array transducer in order to focus through the skull were computed, and the focusing procedure was experimentally validated. The promise of such a method is that it could find application not only in brain tumor hyperthermia, but also in transcranial ultrasonic imaging.

Mention should also be made of recent studies which have used simulation to study the presence of fast and slow modes in trabecular bone according to the Biot theory [28]. For example, Hosokawa [29] and Nagatani *et al.* [30] have used FDTD methods to investigate the sensitivity of the fast and slow modes to various mass and structural parameters of trabecular bone. These studies aim to use additional information contained in the received signal to estimate bone strength, and ultimately fracture risk. Finally, limitations of space prevent discussion of other recent simulation studies in bone but they are cited in the references for the sake of completeness [31]–[33].

IV. Discussion and Conclusion

Simulation in engineering and science has played a key role for decades. Its introduction to ultrasound engineering and research has been much more recent, but it is already having a significant impact. This is true in both industrial nondestructive testing and biomedical applications in general, and with respect to the latter field, particularly true in applications to bone [34]. There are two primary

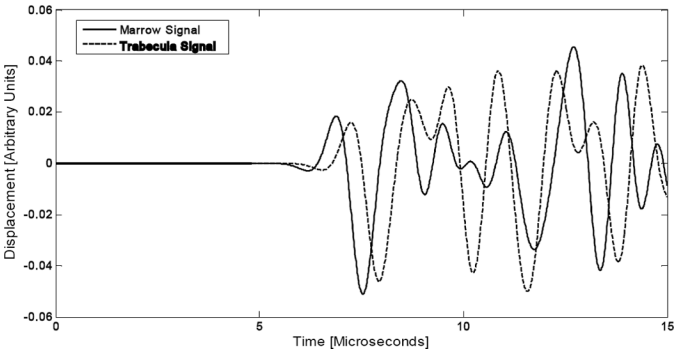

Fig. 20. Simulated time domain waveforms associated with receivers located within marrow only and within a single trabecula. The signal levels are approximately the same.

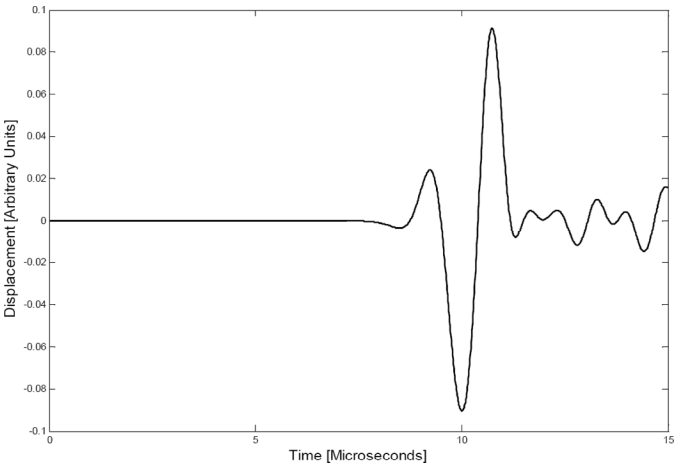

Fig. 21. Simulated time domain waveform associated with the single large through-transmission receiver. Note the reduction in scattered signal component, presumably due to the coherent averaging at the receiver surface.

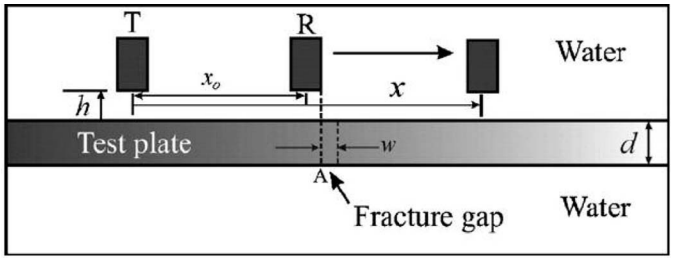

Fig. 22. A geometric representation of the axial transmission apparatus showing the water and test plate, where T and R represent the transmitting and receiving transducers, respectively. x0, x, d, h, and w are the initial transducer separation, transducer separation, test plate thickness, height of the transducer face above the plate, and fracture gap width, respectively. The dotted line above point A represents the starting position of the receiving ultrasound transducer and the arrow shows the direction of receiving transducer motion. Reprinted from *Ultrasound in Medicine and Biology*, vol. 40, Dodd S. P., Cunningham J. L., Miles A. W., Gheduzzi S., Humphrey V. F., "An in vitro study of ultrasound signal loss across simple fractures in cortical bone mimics and bovine cortical bone samples," pp. 656–661, Copyright (2007), with permission from Elsevier.

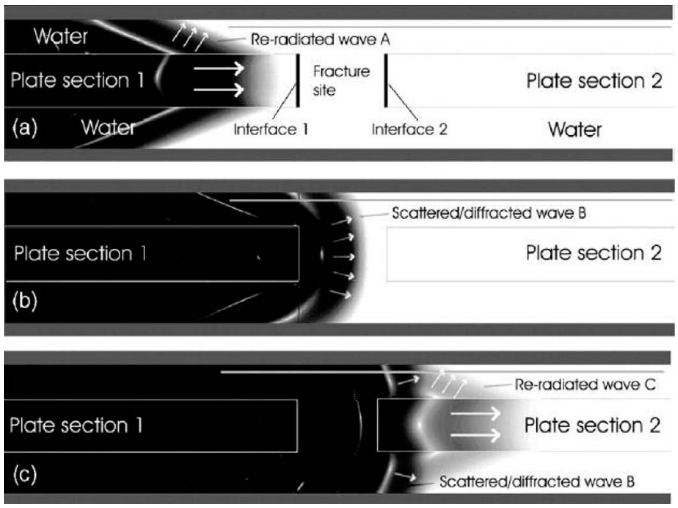

Fig. 23. Snapshots of fracture simulation showing three stages of a 200-kHz wave propagating across a 10-mm fracture gap in a water tank. Sections 1 and 2 represent the two ends of the fracture. Successive dark and light regions of the wave represent the high and low pressure regions of the material, respectively, and the thin grey lines at the top of each picture represent an overlapping array of receiving transducers. Panel (a) shows the plate wave propagating in Section 1 from left to right approaching the fracture site, which produces a re-radiated wave A propagating in the water at a different angle (three white arrows) to the plate wave (two white arrows); panel (b) shows the wave transmitted into the fracture site, denoted by B; and panel (c) shows the wave transmitted into Section 2, which produces the re-radiated wave C. Reprinted from *Ultrasound in Medicine and Biology*, vol. 40, Dodd S. P., Cunningham J. L., Miles A. W., Gheduzzi S., Humphrey V. F., "An in vitro study of ultrasound signal loss across simple fractures in cortical bone mimics and bovine cortical bone samples," pp. 656–661, Copyright (2007), with permission from Elsevier.

reasons for this. The first is the lack of analytic solutions to most problems of interest. Because of the high degree of complexity of the visco-elastic wave equation, and the non-regular geometry and highly heterogeneous nature of bone, analytic solutions to even the most straightforward types of problems are simply not available [35]. This lack of available analytic solutions means that the only recourse (aside from a computational one) is to carry out physical experiments (i.e., *in vitro*, *in vivo*, *in situ*, or clinical). Because these experiments are either excessively costly and time consuming, or indeed impossible to carry out, the potential utility of computational methods is considerable. This leads to the second key reason why simulation has gained so much traction, particularly with respect to bone applications. It is because of the ability to create and/or manipulate "bone specimens" that have specified values of any given property or set of properties. This allows one, for example, to explore variables associated with the biomechanical integrity of bone and correlate them with a number of measured ultrasound parameters. The importance of this aspect cannot be understated because it allows, using computer simulations, the investigation of new techniques for bone assessment and, by immediate extension, for therapy as well. There are virtually an unlimited number of experimental variables that can be manipulated in ultra-

sound interactions with bone and which, through ultrasound simulations, can serve to address an extremely wide variety of questions. The variables include those related to bone (e.g., density, volume fraction, mineralization, marrow properties, architecture, geometry, and biomechanical stiffness and strength) and to the system (e.g., operation in pulse-echo or through-transmission, frequency, bandwidth, signal shape, single element or phased array, and transducer apodization characteristics). The degree to which simulation can provide greater insight is as broad as the number of problems and questions one may pose.

There are several points that should also be mentioned regarding the potential limitations of ultrasound simulation. The first is that careful attention must always be given to validation. Whether or not a particular simulation can provide useful information must ultimately be tested in physical experiments. These should be carried out as early as feasible in the development process to ensure that the simulation model captures sufficient aspects of the problem. Attention should also be given to whether the simulation model is appropriate to the specified problem. For example, all of the simulations presented here utilized the linear visco-elastic or linear elastic wave equation; thus, any problem in which nonlinear effects are present in any significant amount may not be adequately represented by the output of these linear models [36]. A similar comment can be made with respect to the use of 2-D or 3-D simulations. There are certain cases when a 2-D simulation is sufficient (as with the case of tubular structures previously presented [12]), and others when a 3-D simulation is required to capture a key aspect of the problem. For example, Haïat *et al.* report that 2-D simulation of ultrasound through trabecular bone does not reproduce the empirically observed linear variation with frequency of attenuation, while the 3-D simulation does [20], [37].

One key aspect that has not been discussed is the computational resources that are needed to solve a particular problem. In this regard, the primary limitations are related to the memory and computational time required in 3-D problems. For example, in a 3-D ultrasound simulation with a cubic object 1 cm on a side, with a minimum relevant wavelength of 1 mm, memory required would be about 40 MB and a computation time of less than an hour with a typical desktop PC. Additional details are beyond the scope of this paper, but suffice it to say that with the advent of increasingly higher capacity memory chips, 64-bit operating systems, and multi-core processors, memory and computational limitations will over time become less important.

It should be noted again that, although we have primarily presented simulations that rely on the finite difference time domain method, the finite element method can also be utilized [38]. For many, the FDTD method is more attractive as it can be easier to implement. FEM is attractive because of its ability to handle complex geometries (and boundaries) more easily than the FDTD. For example, Protopappas used the FEM to assess guided wave propagation in long bones, and with it was able to model their irregular geometry [26]. It should be noted that the FDTD method could be considered as a special case of the FEM approach, with the appropriate choice of basis functions and element shapes in FEM.

Some additional limitations should be mentioned. Simulation studies to date have not taken into account the anisotropic nature of bone. Although representing an additional computational burden, anisotropic materials can readily be incorporated into the numerical methods discussed. Thus, future simulation studies will need to incorporate this important property in order to more accurately model the propagation of ultrasound in bone. We also have not discussed k-space, ray tracing, or other approximate methods for solving the lossy elastic wave equation [39], [40]. Further, no discussion of two key aspects of computer simulation, namely, stability and numerical error, was provided; the reader is encouraged to consult the literature for additional information on these important topics [41]. Finally, there was little discussion about biophysical and biomechanical material constants for bone and soft tissue. At the minimum, one would need to know the density, the first and second Lamé constants, and the first and second viscosities. Alternatively, one can use knowledge of the density and shear and longitudinal velocities and attenuations to set appropriate values for the Lamé constants and viscosities. This is clearly an important consideration in all computer simulations, and tissue and material data can be found in the excellent compilations of Selfridge [42] and Goss [43], [44].

In conclusion, computer simulation is a valuable tool for studying ultrasound interactions with bone. There are numerous questions and problems that can be modeled and studied using simulation methods. As such, ultrasound simulation is expected to become even more widely used as computers become more powerful and as interest in ultrasound diagnosis and therapy of bone expands as well.

Acknowledgments

The funders had no role in the design and conduct of the study; collection, management, analysis, and interpretation of the data; and preparation, review, or approval of the manuscript. We gratefully acknowledge the assistance of Professor Jose Marcos Alves for the micro-CT image data, and Benjamin Blazy for the simulation and experimental data on the plastic tubes and rods.

References

[1] Anonymous, "Osteoporosis prevention, diagnosis, and therapy," *JAMA*, vol. 285, pp. 785–795, 2001.

[2] J. Kanis, "Diagnosis of osteoporosis and assessment of fracture risk," *The Lancet*, vol. 359, pp. 1929–1936, 2002.

[3] C. W. Miller, "Survival and ambulation following hip fracture," *J. Bone Joint Surg.*, vol. 60A, pp. 930–934, 1978.

[4] L. J. Melton, III, "Epidemiology of fractures," in *Osteoporosis: Etiology, Diagnosis, and Management*. B. L. Riggs and L. J. Melton, III, Eds. New York: Raven Press, 1988, pp. 133–154.

[5] J. J. Kaufman and R. S. Siffert, "Non-invasive assessment of bone integrity," in *Bone Mechanics Handbook*. S. Cowin, Ed. Boca Raton, FL: CRC Press, 2001, pp. 34.1–34.25.
[6] O. Johnell, J. A. Kanis, A. Oden, H. Johansson, C. De Laet, P. Delmas, J. A. Eisman, S. Fujiwara, H. Kroger, D. Mellstrom, P. J. Meunier, L. J. Melton, III, T. O'Neill, H. Pols, J. Reeve, A. Silman, and A. Tenenhouse, "Predictive value of BMD for hip and other fractures," *J. Bone Miner. Res.*, vol. 20, pp. 1185–1194, 2005.
[7] G. M. Blake and I. Fogelman, "Review—DXA scanning and its interpretation in osteoporosis," *Hosp. Med.*, vol. 64, pp. 521–525, 2003.
[8] R. S. Siffert and J. J. Kaufman, "Ultrasonic bone assessment: 'The time has come'," *Bone*, vol. 40, pp. 5–8, 2007.
[9] J. J. Kaufman and T. E. Einhorn, "Review—Ultrasound assessment of bone," *J. Bone Miner. Res.*, vol. 8, pp. 517–525, 1993.
[10] J. L. Rose, *Ultrasonic Waves in Solid Media*. Cambridge, UK: Cambridge University Press, 1999.
[11] B. A. Auld, *Acoustic Fields and Waves in Solids*. 2nd ed. vol. 1, Malabar, FL: Krieger Publishing Company, 1990.
[12] J. J. Kaufman, G. M. Luo, B. Blazy, and R. S. Siffert, "Quantitative ultrasound assessment of tubes and rods: Comparison of empirical and computational results," in *Acoustical Imaging*. vol. 29, I. Akiyama, Ed. New York: Springer, to be published.
[13] B. S. Robinson and J. F. Greenleaf, "Measurement and simulation of the scattering of ultrasound by penetrable cylinders," in *Acoustical Imaging*. vol. 13, M. Kaveh, R. K. Mueller, and J. F. Greenleaf, Eds. New York: Plenum Press, 1984, pp. 163–178.
[14] P. P. Delsanto, R. S. Schechter, H. H. Chaslekis, R. B. Mignogna, and R. Kline, "Connection machine simulation of ultrasonic wave propagation in materials. II: The two-dimensional case," *Wave Motion*, vol. 20, pp. 295–314, 1994.
[15] R. S. Schechter, H. H. Chaslekis, R. B. Mignogna, and P. P. Delsanto, "Real-time parallel computation and visualization of ultrasonic pulses in solids," *Science*, vol. 265, pp. 1188–1190, 1994.
[16] G. M. Luo, J. J. Kaufman, A. Chiabrera, B. Bianco, J. H. Kinney, D. Haupt, J. T. Ryaby, and R. S. Siffert, "Computational methods for ultrasonic bone assessment," *Ultrasound Med. Biol.*, vol. 25, pp. 823–830, 1999.
[17] J. J. Kaufman, G. M. Luo, and R. S. Siffert, "A portable real-time bone densitometer," *Ultrasound Med. Biol.*, vol. 33, no. 9, pp. 1445–1452, 2007.
[18] S. L. Bonnick, *Bone Densitometry in Clinical Practice*. Totowa, NJ: Humana Press, 2004.
[19] E. Bossy, M. Talmant, and P. Laugier, "Three-dimensional simulations of ultrasonic axial transmission velocity measurement on cortical bone models," *J. Acoust. Soc. Amer.*, vol. 115, no. 5, pp. 2314–2324, 2004.
[20] G. Haïat, F. Padilla, F. Peyrin, and P. Laugier, "Variation of ultrasonic properties with microstructure and material properties of trabecular bone: A 3-D model simulation," *J. Bone Miner. Res.*, vol. 22, no. 5, pp. 665–674, 2007.
[21] E. Bossy, F. Padilla, F. Peyrin, and P. Laugier, "Three-dimensional simulation of ultrasound propagation through trabecular bone structures measured by synchrotron microtomography," *Phys. Med. Biol.*, vol. 50, pp. 5545–5556, 2005.
[22] R. S. Siffert and J. J. Kaufman, "Acoustic assessment of fracture healing: Capabilities and limitations of 'a lost art'," *Amer. J. Ortho.*, vol. 25, no. 9, pp. 614–618, 1996.
[23] G. T. Anast, T. Fields, and I. M. Siegel, "Ultrasonic technique for the evaluation of bone fractures," *Am. J. Phys. Med.*, vol. 37, pp. 157–159, 1958.
[24] E. Maylia and L. D. M. Nokes, "The use of ultrasonics in orthopedics—A review," *Technol. Health Care*, vol. 7, no. 1, pp. 1–28, 1999.
[25] S. P. Dodd, J. L. Cunningham, A. W. Miles, S. Gheduzzi, and V. F. Humphrey, "An in vitro study of ultrasound signal loss across simple fractures in cortical bone mimics and bovine cortical bone samples," *Bone*, vol. 40, pp. 656–661, 2007.
[26] V. C. Protopappas, D. I. Fotiadis, and K. N. Malizos, "Guided ultrasound wave propagation in intact and healing long bones," *Ultrasound Med. Biol.*, vol. 32, no. 5, pp. 693–708, 2006.
[27] J.-F. Aubry, M. Tanter, M. Pernot, J.-L. Thomas, and M. Fink, "Experimental demonstration of noninvasive transskull adaptive focusing based on prior computed tomography scans," *J. Acoust. Soc. Amer.*, vol. 113, no. 1, pp. 84–93, 2003.
[28] Z. E. A. Fellah and J. Y. Chapelon, "Ultrasonic wave propagation in human cancellous bone: Application of Biot theory," *J. Acoust. Soc. Amer.*, vol. 116, no. 1, pp. 61–73, 2004.
[29] A. Hosokawa, "Effect of trabecular irregularity on fast and slow wave propagations through cancellous bone," *Jpn. J. Appl. Phys.*, vol. 46, no. 7B, pp. 4862–4867, 2007.
[30] Y. Nagatani, H. Imaizumi, T. Fukuda, M. Matsukawa, Y. Watanabe, and T. Otani, "Applicability of finite-difference time-domain method to simulation of wave propagation in cancellous bone," *Jpn. J. Appl. Phys.*, vol. 45, no. 9A, pp. 7186–7190, 2006.
[31] C. Baron, M. Talmant, and P. Laugier, "Effect of porosity on effective diagonal stiffness coefficients (c_{ii}) and elastic anisotropy of cortical bone at 1 MHz: A finite difference time domain study," *J. Acoust. Soc. Amer.*, vol. 122, no. 3, pp. 1810–1817, 2007.
[32] P. Moilanen, M. Talmant, V. Bousson, P. H. F. Nicholson, S. Cheng, J. Timonen, and P. Laugier, "Ultrasonically determined thickness of long cortical bones: Two-dimensional simulations of in vitro experiments," *J. Acoust. Soc. Amer.*, vol. 122, no. 3, pp. 1818–1826, 2007.
[33] E. Bossy, P. Laugier, F. Peyrin, and F. Padilla, "Attenuation in trabecular bone: A comparison between numerical simulation and experimental results in human femur," *J. Acoust. Soc. Amer.*, vol. 122, no. 4, pp. 2469–2475, 2007.
[34] J. J. Kaufman, G. M. Luo, B. Bianco, A. Chiabrera, and R. S. Siffert, "Computational methods for NDT," in *Proc. SPIE: Nondestructive Evaluation of Aging Materials and Composites III*. vol. 3585, G. Y. Baaklini, C. A. Lebowitz, and E. S. Boltz, Eds. 1999, pp. 173–181.
[35] A. Ishimaru, *Wave Propagation and Scattering in Random Media*. Piscataway, NJ: IEEE Press, 1997.
[36] F. A. Duck, "Nonlinear acoustics in diagnostic ultrasound," *Ultrasound Med. Biol.*, vol. 28, no. 1, pp. 1–18, 2002.
[37] C. M. Langton, S. B. Palmer, and R. W. Porter, "The measurement of broadband ultrasound attenuation in cancellous bone," *Eng. Med.*, vol. 13, pp. 89–91, 1984.
[38] W. F. Ames, *Numerical Methods for Partial Differential Equations*. 3rd ed. San Diego, CA: Academic Press, 1992.
[39] W. F. Walker and G. E. Trahey, "The application of k-space in medical ultrasound," *IEEE Trans. Ultrason., Ferroelect., Freq. Contr.*, vol. 45, pp. 541–558, 1998.
[40] V. Červený, *Seismic Ray Theory*. Cambridge, UK: Cambridge University Press, 2001.
[41] J. C. C. Strikwerda, *Finite Difference Schemes and Partial Differential Equations*. Philadelphia, PA: Soc. Industr. Appl. Math. (SIAM), 2004.
[42] A. R. Selfridge, "Approximate material properties in isotropic materials," *IEEE Trans. Sonics Ultrason.*, vol. SU-32, pp. 381–394, 1985.
[43] S. A. Goss, R. L. Johnston, and F. Dunn, "Comprehensive compilation of empirical ultrasonic properties of mammalian tissues," *J. Acoust. Soc. Amer.*, vol. 64, pp. 423–457, 1968.
[44] S. A. Goss, R. L. Johnston, and F. Dunn, "Compilation of empirical ultrasonic properties of mammalian tissues. II," *J. Acoust. Soc. Amer.*, vol. 68, no. 1, pp. 93–108, 1980.

Jonathan J. Kaufman was born and raised in Brooklyn, New York, and received his undergraduate degree in electrical engineering at City College of the City University of New York in 1975. His Master's and Ph.D. degrees were obtained from Columbia University in 1978 and 1982, respectively.

Since 1982 Dr. Kaufman has served as consultant to a number of biomedical companies, and was involved with studying the interaction of electromagnetic fields with biological systems and also worked on development of ultrasound technology to accelerate the healing of bone fractures. He has served as an Assistant Clinical Professor of Orthopedics at The Mount Sinai School of Medicine since 1985. He is also the President and CEO of CyberLogic, Inc., a small business in New York City that is involved in the development of novel technologies, primarily

in the area of non-invasive assessment of bone strength and fracture risk. Dr. Kaufman is a co-inventor on twenty-five issued United States Patents.

Gangming Luo received a B.S. degree in applied mechanics from Xi'an Jiao Tong University in 1982, and a M.S. degree in engineering mechanics from Shanghai Jiao Tong University in 1984. In 1994, he received a Ph.D. degree in mechanical engineering from The City University of New York.

He has been working at New York University, School of Medicine since 1995, and also at CyberLogic, Inc., in New York City as Director of Computational Mechanics, since 2001. His research interests include ultrasound bone quality assessment, computer simulation of ultrasound wave propagation and bone remodeling.

Robert S. Siffert was a practicing orthopedic surgeon in New York City for over 50 years. He studied at New York University where he received his B.S. in 1939 and his M.D. in 1943.

He was Chairman of the Department of Orthopedics at The Mount Sinai School of Medicine from 1967 to 1987, where he is now Emeritus Professor and Chair. Dr. Siffert served as a flight surgeon in the China-Burma-India theater during 1944 to 1946 and received four battlestars. He has served on the board of CARE and worked as a volunteer consultant in the development of orthopedic programs in developing countries, including Peru, Haiti, Indonesia, Tunisia, Kenya, and Afghanistan. He was also a Senior Consultant for Disabled Children with the New York City Health Department and a Senior VP for the Easter Seals Society. Dr. Siffert has served on the Advisory Board for Clinical Orthopedics and for American Jouurnal of Orthopedics, and was Chair of the Committee for Handicapped Child of the American Academy of Orthopedic Surgeons. His present activities are focused on translational research in the areas of non-invasive assessment of bone strength and fracture risk in osteoporosis.